JPEDAV (2009) 30:429–434
DOI: 10.1007/s11669-009-9568-0
1547-7037 ©ASM International

Solidification Simulation Using Scheil Model in Multicomponent Systems

Shuang-Lin Chen, Ying Yang, Sinn-Wen Chen, Xiong-Gang Lu, and Y. Austin Chang

(Submitted March 19, 2009; in revised form July 6, 2009)

Solidification paths simulated by Scheil model have been analyzed. Since the Scheil model assumes that the already solidified solid phases are "frozen," the simulated solidification paths must follow the eutectic type paths and cross over the peritectic type boundaries to satisfy the mass balance requirement. Examples are given for comparison between the Scheil simulation results and the experimental observations for alloys in Mo-Ti-Si system.

Keywords calculation, phase diagram, solidification simulation

1. Introduction

We have learnt that in an isobaric binary system two basic types of reactions exist during solidification: eutectic and peritectic. Binary eutectic and peritectic reactions can be easily understood from the binary phase diagrams. However, reactions become much more complex in multi-component systems and it is not so easy to understand the reactions in multi-component systems, even in a ternary system. This article details geometrically the eutectic and peritectic types of reactions in a ternary system during solidification simulation with Scheil model and then extends it to multi-component systems. Examples will be presented to compare the prediction from simulation with experimental results. We start from binary system so that the similarity among binary, ternary, and higher order systems can be revealed.

The phase formation during solidification is a kinetic process. In this article, a simple solidification model, the Scheil model,[1] is employed. The major assumptions in this model are: the solidified phases are "frozen," i.e., no back diffusion is considered in the solid phases; diffusion in liquid phase is so fast that liquid phase always has a uniform composition; and the phase equilibrium between the liquid and solid phases at the local interface is reached. This is a good approximation in substitutional phases such as aluminum and nickel alloys. The isobaric condition is also assumed throughout this article.

This article is an invited paper selected from participants of the 14th National Conference and Multilateral Symposium on Phase Diagrams and Materials Design in honor of Prof. Zhanpeng Jin's 70th birthday, held November 3-5, 2008, in Changsha, China. The conference was organized by the Phase Diagrams Committee of the Chinese Physical Society with Drs. Huashan Liu and Libin Liu as the key organizers. Publication in *Journal of Phase Equilibria and Diffusion* was organized by J.-C. Zhao, The Ohio State University; Yong Du, Central South University; and Qing Chen, Thermo-Calc Software AB.

Shuang-Lin Chen, CompuTherm, LLC, Madison, WI 53719 and School of Materials Science and Engineering, Shanghai University, Shanghai 200072, China; **Ying Yang**, CompuTherm, LLC, Madison, WI 53719; and **Xiong-Gang Lu**, School of Materials Science and Engineering, Shanghai University, Shanghai 200072, China; **Sinn-Wen Chen**, Department of Chemical Engineering, National Tsing Hua University, Hsinchu, Taiwan, ROC; **Y. Austin Chang**, Department of Materials Science and Engineering, University of Wisconsin, Madison, WI 53706, USA. Contact e-mail: chang@engr.wisc.edu.

2. Binary Systems

Solidification path in a binary system is simple and straightforward. During a solidification process, the liquid composition proceeds along the liquidus and ends at a local minimum of the liquidus. The possible minima in a binary system are a eutectic, a low congruent melting alloy, and a lower melting component element.

Figure 1 shows two hypothetical binary systems: *A-B* with a peritectic reaction at 647 K and *A-C* with a eutectic reaction at 820.2 K. The melting point temperatures of components in the phases in these two systems are listed in Table 1. The *L*, α, and β phases in both systems are assumed to be ideal solutions with a fusion entropy of 10 J/K. Using an *A-B* alloy with $x_B = 0.5$ as an example, a solidification simulation using the Scheil model predicts the solidification path as the primary α phase followed by the solidification of the β phase. The liquid composition follows the liquidus line during solidification shown as the thicker line in Fig. 1(a). Before the liquid composition reaches the peritectic composition, the primary α phase is solidified. Then, the solidification of the β phase continues until the liquid composition arrives at the melting point of component *B*, where any remain of the liquid transforms into pure solid *B*. The simulated reaction sequence for this solidification is $L \rightarrow \alpha$ (768-647 K) and $L \rightarrow \beta$ (647-600 K). Since the Scheil model assumes that the solidified phases are "frozen," the solidified α phase is not allowed to react with the liquid to form the β phase. Therefore, the peritectic reaction $L + \alpha \rightarrow \beta$ (647 K) does not happen in the solidification simulation using Scheil model. For an *A-C* alloy with $x_C = 0.5$, the predicted solidification path is the primary

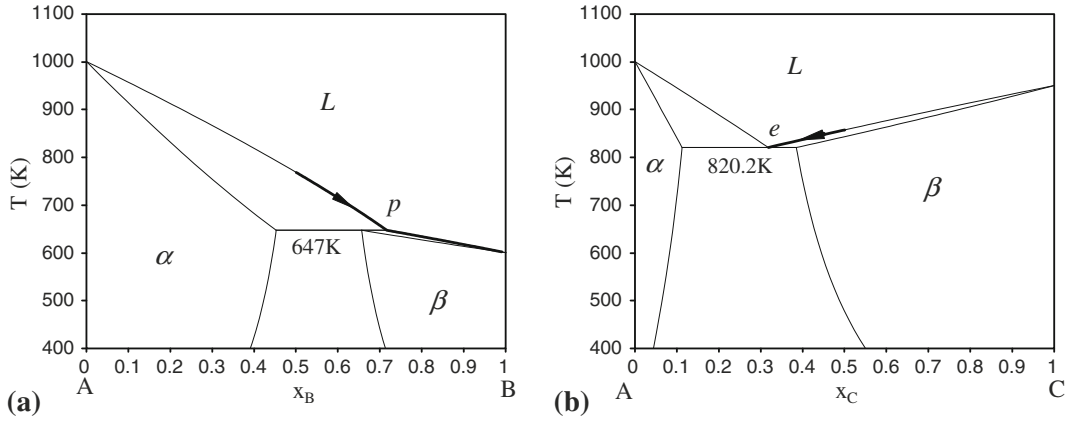

Fig. 1 Binary systems: *A-B* (peritectic) and *A-C* (eutectic). Thicker lines represent the solidification paths of the liquid phases with $x_A = 0.5$. (a) *A-B* system; (b) *A-C* system

Table 1 The melting temperatures of the components for the phases in a hypothetical system *A-B-C*

	Temperature, K		
Phase	**A**	**B**	**C**
α	1000	400	110
β	750	600	950

solidification of the β phase and followed by the eutectic solidification of α + β, as shown as a thicker line in Fig. 1(b). The reaction sequence of solidification simulation for this *A-C* alloy is $L \rightarrow \beta$ (857-820.2 K) and $L \rightarrow \alpha + \beta$ (820.2 K).

The solidification for a binary alloy is easily understood from its temperature-composition phase diagram. With the Scheil model, the solidified phases at any temperature can be easily identified. However, the solidification of a ternary alloy is more complex and will be discussed in the following.

3. Ternary Systems

In the previous section we presented two binary systems *A-B* and *A-C*. A third binary system *B-C* is assumed to have the stable phases *L* and β only and the melting points of the components are the same as those in *A-B* and *B-C* systems, as listed in Table 1. The calculated phase diagram *B-C* is shown in Fig. 2 with a cigar-shaped solid β/*L* phase boundaries. Combination of these three binaries forms a ternary system *A-B-C*, which has three phases: *L*, α, and β. We further assume that these three phases are ideal solutions in the ternary. This system is similar to the model system given in Rhines's book (p. 144).[2] Next we will start from this ternary liquidus projection to analyze the solidification simulation in this system with the Scheil model.

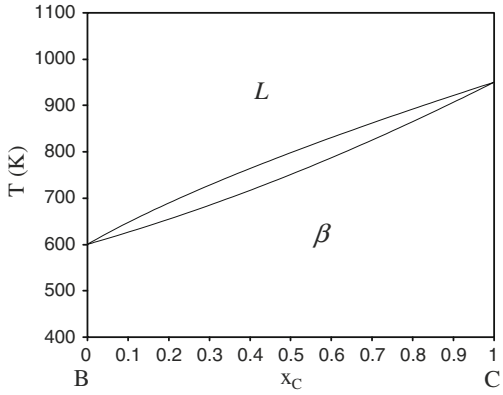

Fig. 2 Binary system *B-C*

3.1 Liquidus Projection

Figure 3(a) and (b) shows the calculated liquidus projection of *A-B-C* and Fig. 3(b) has the calculated isothermal lines (in dashed lines). Since all the three phases are ideal solutions, the isothermal lines are exact straight lines.[3] The monovariant liquidus decreases in temperature from the binary eutectic *e* in *A-C* to the binary peritectic *p* in the binary *A-B*. In the *A*-rich side, the primary phase of solidification is α while in the *A*-poor side β. In contrast to binary alloys *e* and *p* which solidify isothermally, the ternary liquid alloys along this monovariant liquidus solidify as a function of temperature due to one more degree of freedom. Starting from alloy *e*, the Scheil solidification is eutectic-like but eventually must change to peritectic-like with decrease in temperature. In the present case, it is at the point "*t*" as shown in Fig. 3(b); the temperature and composition of the alloy at this transition point are 683.7 K and $x_A = 0.358$, $x_B = 0.583$, and $x_C = 0.059$. Subsequent Scheil solidification of the alloys along the monovariant liquidus at lower temperatures is peritectic-like. In other words, the solidified microstructures differ for the alloys in the different sides of the transition point "*t*" on the monovariant liquidus line.

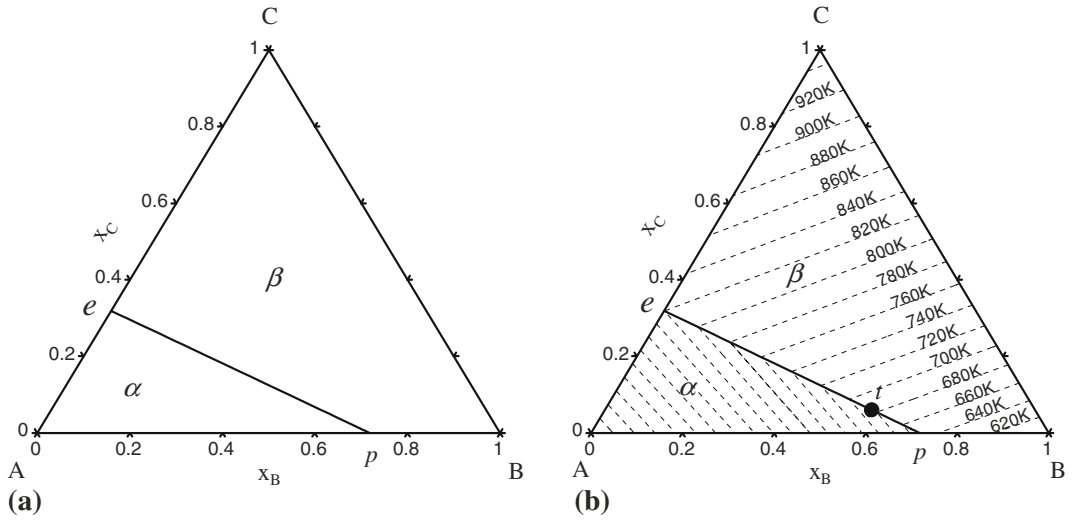

Fig. 3 Liquidus projection of *A-B-C* (a) without isothermal lines; (b) with isothermal lines

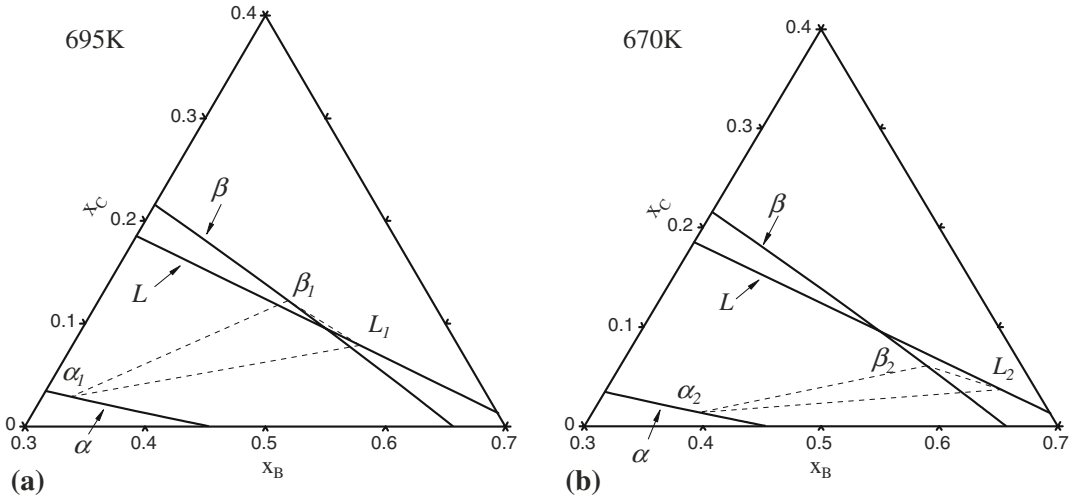

Fig. 4 Projections of the monovariant lines for the three phases with tie-triangles at two temperatures. (a) Eutectic at 695 K; (b) Peritectic at 670 K

It should be noted that the existence of a unique transition point "*t*" is valid only if we consider the phase equilibrium for the overall composition of the homogeneous liquid phase in current step and all the already solidified solid phases in previous steps are considered "frozen" and do not participate in the current equilibrium. Next, we will demonstrate how to determine this point.

3.2 Transition from Eutectic-like Reaction to Peritectic-like Reaction on Monovariant Line

We normally describe an invariant reaction as a reaction equation. For example, in a previous article[4] we described how to calculate the invariant reaction equations, which has been implemented in Pandat, a software package for multi-component phase equilibrium calculation.[5-7] Pandat also calculates the reaction equations for non-invariant reactions.

In Fig. 3(b), the reaction along the monovariant line (*ep*) of the liquid phase changes from a eutectic one to a peritectic one at point "*t*" with $T = 683.7$ K. For a better understanding of this transition, two tie-triangles, L_1-α_1-β_1 above the transition temperature (683.7 K) and L_2-α_2-β_2 below it, are shown as dashed triangles in Fig. 4(a) and (b) at 695 K and 670 K, respectively. The solid lines plotted in Fig. 4(a) and (b) are the projections of the monovariant lines of the liquid, α and β phases, i.e., the liquidus line (*L*) and the two solidus lines (α and β). It seems that the liquidus and the β solidus crosses at the point. In reality, the liquidus and solidus of the same three-phase equilibrium never intersect with each other in the composition-temperature space.

Figure 4(a) shows that at 695 K the intersection point between the monovariant liquidus *L* and the tie-line $\alpha_1\beta_1$ is on the tie-line $\alpha_1\beta_1$. Therefore, the reaction is of eutectic

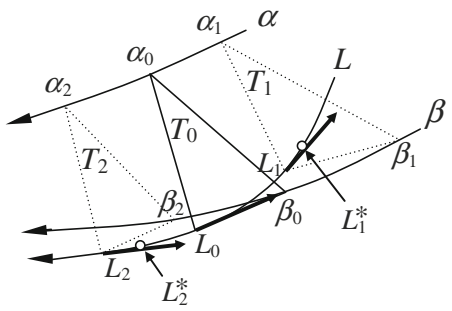

Fig. 5 A schematic liquidus projection diagram showing the transition between eutectic and peritectic reaction. The thicker lines are the tangents to the liquidus L

type. However, Fig. 4(b) shows that at 670 K the intersection point between the liquidus L and the tie-line $\alpha_2\beta_2$ falls on the extension of the tie-line $\alpha_2\beta_2$. That means the reaction type at 670 K is of peritectic. Since the monovariant liquidus line and the two solidus lines are very close to straight lines, Fig. 4 does not tell us the key point how to determine a reaction type in a more general situation. A curved liquidus invariant line is presented below for this purpose.

Figure 5 is a schematic diagram illustrating the relative position change of the tie-triangles and monovariant lines from a eutectic reaction to a peritectic one. Three tie-triangles are plotted: $L_1\alpha_1\beta_1$ at T_1, $L_0\alpha_0\beta_0$ at T_0, and $L_2\alpha_2\beta_2$ at T_2 with $T_1 > T_0 > T_2$. A eutectic reaction occurs at T_1 and a peritectic at T_2. T_0 represents a transition temperature at which the eutectic reaction transforms to a peritectic one. The arrows of the monovariant lines point to the direction of decreasing temperature. The tangent lines to liquidus at L_1, L_0, and L_2 are plotted as the thicker arrows. It can be seen that the tangent line at T_1 passes through the tie-triangle $L_1\alpha_1\beta_1$. If the previous simulation step T_1^* and the current step T_1 are close enough $(T_1^* > T_1)$, the liquid composition L_1^* at T_1^* should be close enough to L_1 and must be inside the tie-triangle $L_1\alpha_1\beta_1$ on the projection plane. At T_1, α_1, and β_1 will solidify from L_1^* and the remaining liquid will be at L_1. Mass redistribution to the three phases in this way satisfies the mass balance condition and the reaction at T_1 is of eutectic. Let's look at the tie-triangle $L_2\alpha_2\beta_2$ at T_2. The tangent line to liquidus at L_2 does not go into $L_2\alpha_2\beta_2$. Using the same argument as above, if the previous simulation step T_2^* and the current step T_2 are close enough $(T_2^* > T_2)$, the liquid composition L_2^* at T_2^* should be also close enough to L_2. Since on the projection plane the tangent is outside of $L_2\alpha_2\beta_2$, L_2^* must be outside $L_2\alpha_2\beta_2$, too. From the relative positions of L_2^* and $L_2\alpha_2\beta_2$, the reaction at T_2 is a peritectic, $L + \alpha \rightarrow \beta$. At T_0, the tangent line to the liquidus at L_0 coincides with the side $L_0\beta_0$ of the tie-triangle $L_0\alpha_0\beta_0$. This tangent line is neither inside the tie-triangle and nor outside. Therefore, at this temperature, the reaction type changes from eutectic to peritectic, i.e., a transition point.

It should be emphasized again that above discussion is based upon the assumption in Scheil model that the phase equilibrium considered is for the overall composition of the current homogeneous liquid on the liquidus surface. For the lever rule model, the situation is different. Kevorkov et al.[8] have found that the transition point in lever rule simulation may vary with the overall composition of the system.

3.3 Scheil Simulation with Eutectic-like and Peritectic-like Monovariant Reactions

Two examples in the hypothetical *A-B-C* ternary described above are used to analyze the solidification paths. Choose an alloy with $x_A = 0.7$, $x_B = 0.15$, and $x_C = 0.15$ as the first example. Figure 6(a) shows the solidification path with the Scheil model overlaid on the liquidus surface. The primary phase α solidifies first at 838.4 K. The liquid phase composition changes with decreasing temperature. The path reaches the monovariant liquidus at 776.0 K with the liquidus composition of $x_A = 0.569$, $x_B = 0.202$, and $x_C = 0.229$, where the reaction is a eutectic type ($L \rightarrow \alpha + \beta$) Since the eutectic reaction satisfies the mass balance condition in the Scheil model, the eutectic solidification will continue to follow the monovariant line until the transition point "*t*" from eutectic to peritectic. The liquid composition at "*t*" does not fall into the tie-triangle at a lower temperature and a peritectic reaction is expected. However, since the Scheil model does not allow back diffusion from solid back to liquid, the liquid composition no longer follows the monovariant liquidus due to the mass balance constraint. The path of solidification departs from the monovariant liquidus at point "*t*"; it subsequently enters into the compositional region with β as the primary phase of solidification and eventually ends at the pure component *B*.

Another example is an alloy with $x_A = 0.4$, $x_B = 0.15$, and $x_C = 0.45$. This alloy has primary solidified phase of β. As shown in Fig. 6(b), solidification starts at 829.4 K and reaches the monovariant liquidus at 737.8 K with the composition of $x_A = 0.478$, $x_B = 0.367$, and $x_C = 0.155$, which is also a eutectic type of reaction. The subsequent path of solidification is identical to that of the previous example and the final solidification ends at the pure component *B*. For this alloy, the primary phase of solidification is β and the last solidified is also β. In the middle stage, a eutectic-like mixture of α and β is formed.

4. Scheil Simulation in Multi-Component Systems

An understanding of the paths of solidification of ternary alloys using the Scheil simulation is helpful to comprehend those for higher order alloys. Since the Scheil model assumes that the already formed solid phases are "frozen," subsequent simulation focuses on the solidification of the remaining liquid. This assumption requires that at each simulation step the newly formed solid and liquid phases, which are in equilibrium, must have the mass balance with the remaining liquid in the previous step. This mass balance requirement forces the solidification path goes through eutectic types of reactions, i.e., only the paths with eutectic reaction types, such as $L \rightarrow \alpha$, $L \rightarrow \alpha + \beta$, and $L \rightarrow \alpha + \beta + \cdots$, are allowed. Scheil simulation never goes along a peritectic-like reaction path such as $L + \alpha \rightarrow \beta + \gamma$ and $L + \alpha \rightarrow \beta + \gamma + \delta$. If a non-eutectic reaction is met, Scheil

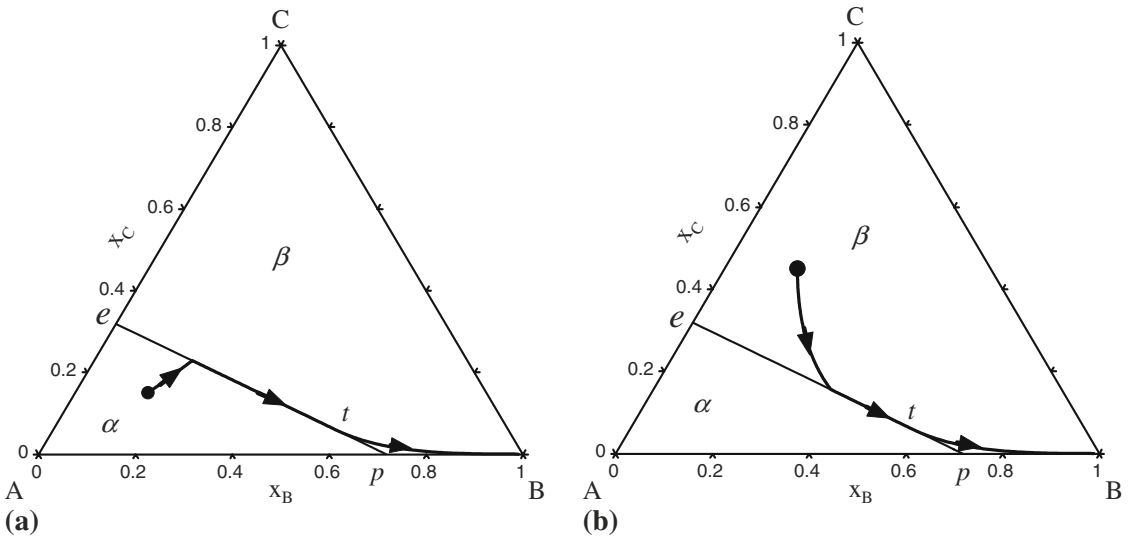

Fig. 6 Liquidus projection of *A-B-C* with Scheil solidification paths of two ternary alloys. (a) Alloy of $x_B = 0.15$ and $x_C = 0.15$; (b) Alloy of $x_B = 0.15$ and $x_C = 0.45$

simulation will automatically cross over it. It is noted that since Scheil simulation follows the paths of eutectic types of $L \rightarrow \alpha + \cdots$ and crosses over the peritectic types of $L + \alpha \rightarrow \beta + \cdots$, it does not fall into a peritectic type of $L + \alpha + \beta \rightarrow \gamma + \cdots$, unless a degenerate case happens. An example of Scheil simulation for a quaternary system Al-Mg-Cu-Si can be found in Chang.[9]

5. Examples

Two alloys in the Mo-Si-Ti ternary system are chosen to compare the Scheil simulation results with the experimental observation.

The liquid-solid phase equilibria of the Mo-Si-Ti system were investigated for development of high-temperature Mo-Si-B-Ti alloys. Detailed experimental investigation and thermodynamic modeling can be found elsewhere.[10] Figure 7 shows the calculated liquidus projection of the Mo-Si-Ti system. The solid lines are the monovariant liquidus lines on the liquidus surface and the thicker lines represent the simulated solidification paths of two alloys using the Scheil model. Alloy "1" has a composition of Mo-0.1Ti-0.3Si and alloy "2" Mo-0.23Ti-0.32Si (both in mole fraction). The label "*t*" denotes a transition point from the eutectic reaction $L \rightarrow Mo_5Si_3 + Mo_3Si$ for Mo-rich alloys to the peritectic reaction $L + Mo_5Si_3 \rightarrow Mo_3Si$ on the right hand side. The primary phase of Scheil solidification of alloy "1" is Mo_5Si_3 followed by eutectic solidification of $Mo_5Si_3 + Mo_3Si$, ending in the binary Mo-Si. During the eutectic solidification, the liquid composition stays on the monovariant eutectic valley of $L \rightarrow Mo_5Si_3 + Mo_3Si$ until the binary eutectic. On the other hand, alloy "2" starts with the primary solidification of Mo_5Si_3. When the liquid composition reaches the monovariant liquidus of the peritectic type, the liquid composition

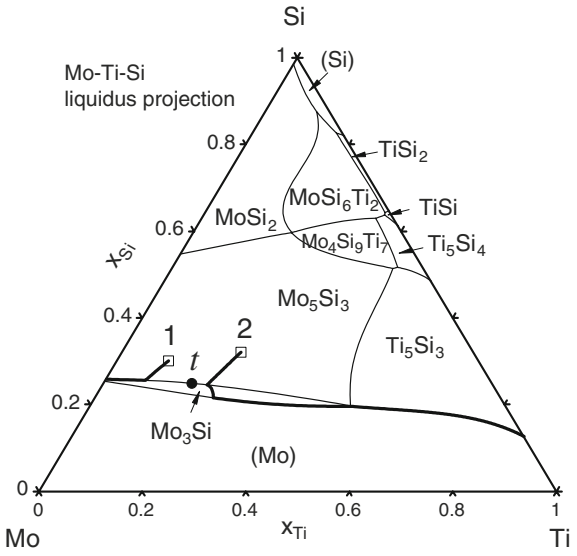

Fig. 7 Calculated liquidus projection of Mo-Si-Ti system. The solid lines are the monovariant liquidus lines and the thicker lines the simulated solidification paths of alloy "1" (Mo-0.1Ti-0.3Si) and alloy "2" (Mo-0.23Ti-0.32Si) using Scheil model[10]

does not stay on the monovariant line, instead it goes into the primary solidification region of Mo_3Si. Then, the Mo_3Si phase is solidified until the liquid composition reaches another eutectic valley of $L \rightarrow (Mo) + Mo_3Si$. The subsequent solidification stays on the eutectic valley of $L \rightarrow Mo_3Si + (Mo)$ and eventually follows the eutectic valley of $L \rightarrow Ti_5Si_3 + (Mo)$.[10] The Scheil simulation predicts the mole fraction of the solid phase resulted from the primary solidification of Mo_5Si_3 and Mo_3Si is more than 95%, which indicates the final solidified eutectic of $Mo_3Si + (Mo)$ and $Ti_5Si_3 + (Mo)$ may not be easily

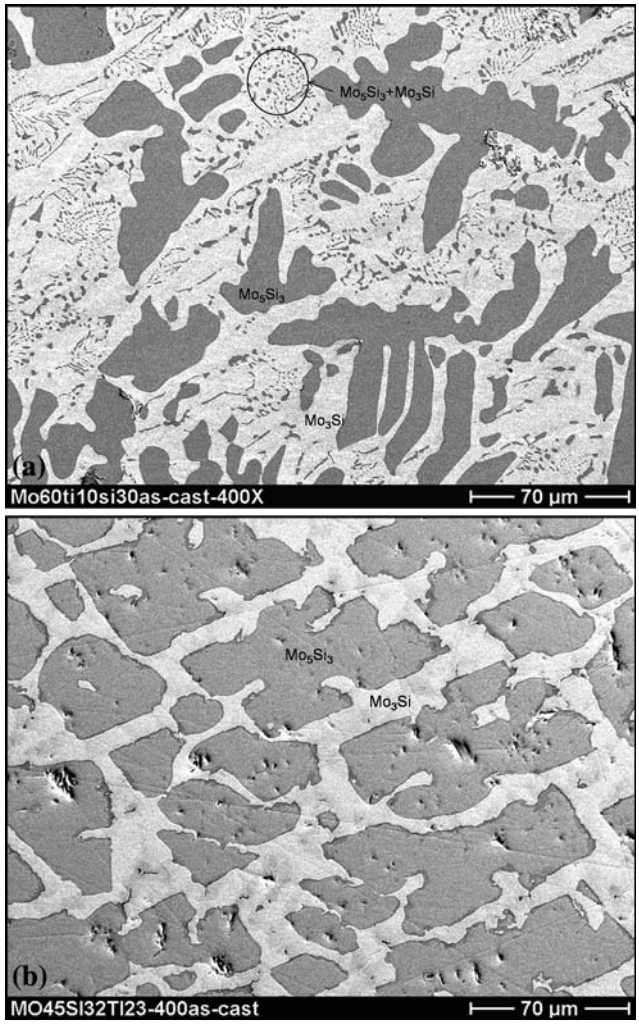

Fig. 8 BSE images of as-cast microstructure: the dark gray phase is Mo_5Si_3 and the light gray Mo_3Si. (a) Alloy 1: Mo-0.1Ti-0.3Si; (b) Alloy 2: Mo-0.23Ti-0.32Si

detected from experimental study of the solidified alloy "2". Figure 8(a) and (b) shows the as-cast microstructures of alloys "1" and "2", respectively, using Scanning Electron Microscopy (SEM) in Back Scattered Electron (BSE) Image mode. As-cast microstructure of alloy "1" is featured by the Mo_5Si_3 primary dendrite and the eutectic of Mo_3Si + Mo_5Si_3 in between the primary dendrites. In alloy "2", no eutectic of Mo_3Si + Mo_5Si_3 was observed. This alloy is featured by the solidification of Mo_5Si_3 followed by the solidification of Mo_3Si. This example demonstrates that the Scheil simulation on solidification path is a very useful tool to help understand some complicated as-cast microstructures.

6. Conclusion

Solidification paths calculations using the Scheil model have been analyzed using a hypothetical ternary system. It has been shown that the Scheil simulated solidification paths must follow the eutectic type paths ($L \rightarrow \alpha + \beta + \cdots$) and cross over the peritectic type boundaries ($L + \alpha \rightarrow \beta + \cdots$). There are two reasons for taking such a special solidification path: the mass balance requirement and the assumption that the already solidified solid phases are "frozen" and no diffusion in solids is taken into account. The calculated paths of solidifications of two Mo-Ti-Si alloys agree with those obtained experimentally. The present method of calculation can be utilized to calculate the paths of higher order alloys provided that thermodynamic databases are available.

Acknowledgments

Y. A. Chang wishes to acknowledge the financial support of this work from the AFSOR Grant No. FA9550-06-1-0229, the NSF-FRG Grant No. NSF-DMR-06-05662 and the Wisconsin Distinguished Professorship. X.-G. Lu thanks the Ministry of Science and Technology and Education of China and the National Science Foundation of China for their financial support under Contract Nos.: 2006AA06Z124, 2007CB613606 (MOST), NCET-06-0434 (EDU), 50774052 (NSFC).

References

1. E. Scheil, *Z. Metallkd.*, 1942, **34**, p 70-72
2. F.N. Rhines, *Phase Diagrams in Metallurgy*, McGraw-Hill Book Co., New York, 1956
3. S.-L. Chen and Y.A. Chang, The Shapes of the Phase Boundaries of Two Ideal Solution Phases in Ternary and Higher Order Systems, *Metall. Mater. Trans.*, 1994, **25A**(3), p 656-658
4. S.-L. Chen, W. Cao, Y. Yang, F. Zhang, K. Wu, Y. Du, and Y.A. Chang, Calculation and Application of Liquidus Projection, *Rare Metals*, 2006, **25**(5), p 532-537
5. S.-L. Chen, S. Daniel, F. Zhang, Y.A. Chang, X.-Y. Yan, F.-Y. Xie, R. Schmid-Fetzer, and W.A. Oates, The PANDAT Software Package and its Applications, *CALPHAD*, 2002, **26**(2), p 175-188
6. S.-L. Chen, F. Zhang, S. Daniel, F.-Y. Xie, X.-Y. Yan, Y.A. Chang, R. Schmid-Fetzer, and W.A. Oates, Calculating Phase Diagrams Using PANDAT and PanEngine, *JOM*, 2003, **55**(12), p 48-51
7. W. Cao, S.-L. Chen, F. Zhang, K. Wu, Y. Yang, Y.A. Chang, R. Schmid-Fetzer, and W.A. Oates, PANDAT Software with PanEngine, PanOptimization and PanPrecipitation for Materials Property Simulation of Multi-Component Systems, *CALPHAD*, 2009, **33**, p 328-342
8. D. Kevorkov, R. Schmid-Fetzer, and F. Zhang, Phase Equilibria and Thermodynamics of the Mg-Si-Li System and Remodeling of the Mg-Si System, *J. Phase Equilib. Diffus.*, 2004, **25**(2), p 140-151
9. Y.A. Chang, Phase Diagram Calculations in Teaching, Research, and Industry, *Met. Mater. Trans. B*, 2006, **37B**(2), p 7-39
10. Y. Yang, Y.A. Chang, L. Tan, and Y. Du, Experimental Investigation and Thermodynamic Descriptions of the Mo-Si-Ti System, *Mater. Sci. Eng. A*, 2003, **361**(1-2), p 281-293